J Comput Aided Mol Des (2010) 24:659–674
DOI 10.1007/s10822-010-9364-2

Allosteric antagonist binding sites in class B GPCRs: corticotropin receptor 1

Supriyo Bhattacharya · Govindan Subramanian · Spencer Hall · Jianping Lin · Abdelazize Laoui · Nagarajan Vaidehi

Received: 12 February 2010 / Accepted: 3 May 2010 / Published online: 29 May 2010

Abstract The 41 amino acid neuropeptide, corticotropin-releasing factor (CRF) and its associated receptors CRF_1-R and CRF_2-R have been targeted for treating stress related disorders. Both CRF_1-R and CRF_2-R belong to the class B G-protein coupled receptors for which little information is known regarding the small molecule antagonist binding characteristics. However, it has been shown recently that different non-peptide allosteric ligands stabilize different receptor conformations for CRF_1-R and hence an understanding of the ligand induced receptor conformational changes is important in the pharmacology of ligand binding. In this study, we modeled the receptor and identified the binding sites of representative small molecule allosteric antagonists for CRF_1-R. The predicted binding sites of the investigated compounds are located within the transmembrane (TM) domain encompassing TM helices 3, 5 and 6. The docked compounds show strong interactions with H228 on TM3 and M305 on TM5 that have also been implicated in the binding by site directed mutation studies. H228 forms a hydrogen bond of varied strengths with all the antagonists in this study and this is in agreement with the decreased binding affinity of several compounds with H228F mutation. Also mutating M305 to Ile showed a sharp decrease in the calculated binding energy whereas the binding energy loss on M305 to Leu was less significant. These results are in qualitative agreement with the decrease in binding affinities observed experimentally. We further predicted the conformational changes in CRF_1-R induced by the allosteric antagonist NBI-27914. Movement of TM helices 3 and 5 are dominant and generates three degenerate conformational states two of which are separated by an energy barrier from the third, when bound to NBI-27914. Binding of NBI-27914 was predicted to improve the interaction of the ligand with M305 and also enhanced the aromatic stacking between the ligand and F232 on TM3. A virtual ligand screening of $\sim$13,000 compounds seeded with $\sim$350 CRF_1-R specific active antagonists performed on the NBI-27914 stabilized conformation of CRF_1-R yielded a 44% increase in enrichment compared to the initially modeled receptor conformation at a 10% cutoff. The NBI-27914 stabilized conformation also shows a high enrichment for high affinity antagonists compared to the weaker ones. Thus, the conformational changes induced by NBI-27914 improved the ligand screening efficiency of the CRF_1-R model and demonstrate a generalized application of the method in drug discovery.

Keywords Class B GPCR · Corticotropin receptor · CRF1 · Allosteric modulator · Drug design

Electronic supplementary material The online version of this article (doi:10.1007/s10822-010-9364-2) contains supplementary material, which is available to authorized users.

S. Bhattacharya · S. Hall · J. Lin · N. Vaidehi (✉)
Department of Immunology, Beckman Research Institute of the City of Hope, Duarte, CA 91010, USA
e-mail: NVaidehi@coh.org

G. Subramanian · A. Laoui (✉)
Chemical and Analytical Sciences, Sanofi-Aventis, 1041, Route 202-206, Bridgewater, NJ 08807, USA
e-mail: abdelazize.laoui@sanofi-aventis.com

Introduction

The 41 amino acid neuropeptide, corticotropin-releasing factor (CRF) and its associated CRF_1 and CRF_2 receptors (CRF_1-R & CRF_2-R) mediate a wide variety of physiological processes primarily induced by continued stress.

CRF secreted in the hypothalamus activates the CRF_1 or CRF_2 receptors initiating multiple signal transduction pathways that modulate stress related disorders. Several non-peptide antagonists to CRF_1-R have been shown [1] as an effective therapeutic strategy to treat stress related disorders in animal models [1–3], and in early human trials [4, 5]. Moreover, recent studies also highlighted the potential role of CRF_1 receptor antagonists in other indications like drug dependence and withdrawal, as well as irritable bowel syndrome [6]. The therapeutic benefit of small molecule CRF_1 receptor antagonists that demonstrated clinical efficacy [4, 5] suggested the potential druggability of this receptor [7] and therefore pharmaceutical companies are focused on developing small molecule antagonists to target the CRF_1 receptors and treat the postulated disorders. Such a feat would require a comprehensive knowledge and understanding of the receptor binding site and its interaction with known antagonists.

Some of the major challenges posed in elucidating the structural basis of the antagonist binding site for CRF_1 receptor are (a) severe paucity in the structural information for CRF receptors, and in general, for class B G-protein coupled receptors (GPCRs) to which they belong; (b) lack of reliable structural model building for class B GPCRs owing to its poor sequence identity to class A GPCRs; and c) the conformational flexibility of the receptor.

There are crystal structures solved for four different class A GPCRs [8–12] that enable homology modeling of other class A GPCRs based on conserved motif of residues in each TM region. These methods have shown mixed success, yet play an integral role in the rational design of small molecules for lead identification and optimization [13]. On the other hand, modeling class B GPCRs still remains a challenge due to the lack of conserved sequence motifs in the TM regions with class A GPCRs. Therefore, the quality of the homology based models of class B GPCRs is dependent on the arbitrary alignment of class A and class B GPCRs. Furthermore, several point mutation data for CRF_1 receptor suggests that the non-competitive small molecule antagonists prefer binding to the transmembrane (TM) domain of the receptor [14–16], for which there is no structural information.

It has been shown that class A GPCRs exist in multiple active and inactive conformations that become relevant for functional specificity in drug design [17, 18]. Recently, Hoare et al. showed that the allosteric modulators of CRF_1 receptor regulate the conformational states of the receptor, thus providing indirect evidence for multiple conformational states of the receptor [15–19].

In this study, we address the above listed challenges in modeling the antagonist binding site of class B human CRF_1 receptor, denoted as *h*CRF_1-R, hereafter in this manuscript. To address the challenge in modeling class B GPCR, we used the ab initio structure prediction method, MembStruk4.0 [20, 21] that does not depend on the sequence alignment to the class A GPCRs and have also been demonstrated to work well for class A GPCRs [21–23]. Using the structural models developed, we predicted the binding sites and binding modes of representatives from three chemical series and other antagonists (total of 13 antagonists) in *h*CRF_1-R. The predicted binding modes and its associated interaction energy have been correlated with the reported structure–activity data and available site directed mutagenesis data [14, 18, 24, 25]. Since the conformation dynamics and flexibility is very important for drug design and mapping ligand specific state, we used the computational method, *LITiCon* [26, 27], to study the ligand induced conformational changes induced by the antagonist NBI-27914 [28].

Computational methods

MembStruk model of CRF1

The human CRF_1-R structure was modeled using with the MembStruk 4.36 method [20, 21]. The general steps of the MembStruk 4.36 and details specific for the *h*CRF_1-R are described below.

Prediction of the transmembrane (TM) regions—TM2ndS

Location of the seven TM helices were predicted using TM2ndS described in Trabanino et al. [29]. The sequence alignment consisting of 15 secretin-like class B human GPCRs were used for this purpose. These sequences have a sequence identity of 23% or higher.

The final TM prediction for the *h*CRF_1-R was obtained through these steps and is shown below:

NT	1 MGGHPQLRLVKALLLLGLNPVSASLQD QHCESLSLASNISGLQCNASVDLIGTC WPRSPAGQLVVRPCPAFFYGVRYNTTNNG YRECLANGSWAARVNYSECQEIL NEEKKSKVHY 116 (116)
TM 1	117 HVAVIINYLGHCIS**L**VALLVAFVLFLR LRP 146 (30)
ICL 1	147 GCTHWGDQADGALEVGAPWSGAPFQ VRRSIRCLRN 181 (35)
TM 2	182 IIHWNLI**S**AFILRNATWFVVQLTMSP 207 (26)
ECL 1	208 EVHQSNVGWCR 218 (11)
TM 3	219 LVTAAYNYFHVTN**F**FWMFGEGCYLHT AIVLT 249 (31)
ICL 2	250 YSTDRLR 256 (7)

TM 4	257 KWMFICIGWGV**P**FPIIVAWAIG 278 (22)
ECL 2	279 KLYYDNEKCWFGKRPGVY 296 (18)
TM 5	297 TDYIYQGPMILVL**L**INFIFLFNIVRI 322 (26)
ICL 3	323 LMTKLRASTTSETIQYR 339 (17)
TM 6	340 KAVKATLV**L**LPLLGITYMLFFVNPG 364 (25)
ECL 3	365 EDEVSR 370 (6)
TM 7	371 VVFIYFNSFLESFQG**F**FVSVFYCFLN 396 (26)
CT	397 SEVRSAIRK RWHRWQDKHSIR ARVARAMSIPTSPTRVSFHSI KQSTAV 444 (48)

The hydrophobic maximum for each helix that defines a center plane that aligns with the middle of the lipid bilayer was determined using the hydrophobic maximum predicted for each TM helix for rhodopsin. The alignment of rhodopsin to class B CRF_1-R was done based on the hypothesis that functionally important residues in the TM regions of class A peptide GPCRs like the chemokine receptors, could be conserved in class B peptide GPCRs like the CRF_1-R. The hydrophobic maxima predicted for rhodopsin [28] was transferred to CRF_1-R using this alignment. The bold and underlined font residues in Scheme 1 represent the hydrophobic maximum for each helix.

Assembly of the helix bundle

The hydrophobic maximum for each helix specifies the z position of each of the seven helices; the *x*, *y* position is taken from the 7.5Å electron density map of frog rhodopsin [30] by fitting a *x*, *y* plane to the predicted TM maxima in the hydrophobicity for each helix. In addition the tilt of each axis from the *z* axis is taken from this structure. The initial orientation of the helix about this axis is determined by calculating the net hydrophobic moment of the middle one-third of the helix (centered at the hydrophobic center) and pointing it outward from the center of the *xy* positions of the seven helices. These orientations are then optimized as in step 4. After assembling the helices into the bundle, we optimize the side chains using SCWRL3.0 [31].

Optimization of helical kinks

We constructed canonical helices for the predicted TM segments and optimize the structures of the individual helices with energy minimization followed by Cartesian molecular dynamics at constant temperature of 300 K for 200 ps. The lowest energy conformation from the MD trajectory of each helix was matched back into the seven helical template built above. The side chains were reoptimized with SCWRL v3.0, followed by final conjugate gradient energy-minimization of the seven-helix bundle. For the *h*CRF_1-R the helical bend angles are: TM1 12.2°°, TM2 3.6°, TM3 4.0°, TM4 11.5°, TM5 5.4°, TM6 22.3°, TM7 4.0°.

Optimization of the rotational orientation of the helices

The rotational orientation of each helix with respect to the TM bundle is important in determining which residues are inside the bundle. The initial positioning of the helices based on hydrophobic moment (step 2) is followed by the ROTMIN step in which each of the 7 helices is rotated by 5 degrees increment to ±30°, the side chains are recalculated (SCWRL) and the potential energy of the rotated helix in the field of all other helices is minimized. We start this procedure with helix3 and then take the best rotation angle for helix3 and further perform this optimization for helix4, followed by helices 5, 6, 7, 1, and 2. This process goes sequentially through all 7 helices and continues until the orientation of each helix no longer changes. This is the procedure used for the published work so far.

Optimization of the assembled helical bundle in explicit lipids

We embed the optimized helix bundle from step 4 into a lipid bilayer and equilibrate the composite system. Equilibration of the helix bundle plus lipid bilayer system uses Rigid Body Molecular Dynamics [32]. The helix bundle surrounded by lipid bilayers (dilaurylphosphatidylcholine) was optimized using rigid body dynamics with DREIDING force field [33] and CHARMM22 [34] charges for the protein.

Generation of an ensemble of Low energy conformations in MembStruk

This step predicts an ensemble of low energy receptor conformations that is important for GPCRs, since GPCRs conformations are dynamic. We generated alternate low potential energy TM barrel conformations by systematically varying the rotational orientation of each helix by 5° and then optimizing the TM barrel and calculating the total energy of the rotated helix. Each helix of the protein in lipid bilayer of is rotated by +5°, the side chain conformations optimized using SCWRL and the potential energy minimized (0.1 kcal/mol/Å in RMS, 500 steps) and then all but the target helix is fixed and minimized (0.1 kcal/mol/Å in RMS, 800 steps) to obtain a total potential energy. The number of inter-helical HBs and salt bridges formed in each rotated conformation is counted as well. The inter-helical HBs are counted with a distance constraint of 3.5Å

for the length of the HB and angle of 120°. The rotations by 5° is done repeatedly until the helix has been rotated a total of 360° and an energy and HB profile is made for each rotation. Using this information, a set of rotations is chosen based on lowest energies for each helix and the maximum number of inter-helical HBs especially those HBs made by the residues in the middle of the TM helices.

Generation of an ensemble of low energy structures

Next several structures are generated using combination of individual helical minima chosen from step 6, that lead to an ensemble of conformations (all possible combinations from the rotations chosen). Each structure is minimized using conjugate gradients (0.1 kcal/mol/Å in RMS in force, 500 steps) and energies are obtained (fixing the lipids, 800 steps, 0.1 kcal/mol/Å in RMS). The total potential energy of these TM bundle structures is calculated in explicit but finite lipid bilayer. The total number of inter-helical HBs is also calculated. The inter-helical HBs are counted with a distance constraint of 3.5Å for the length of the HB and angle of 120°. The set of structures are sorted by inter-helical HBs and then by total energy. We chose two possible low energy conformations for the *h*CRF_1-R structure with two possible rotations for helices 4 and 5.

Loop addition

Extra- and intracellular loops were added using Modeller 7v7 [35]. The loops once built are energy-minimized (500 steps, CMM level 0) while the rest of the protein is kept fixed. After the energy-minimization, the loop side chains are optimized (SCWRL) and then energy-minimized again (500 steps, CMM level 0). The final protein structures including intra- and extra-cellular loops are then energy-minimized for 5,000 steps with only loops allowed to move; this is followed with the energy-minimization of the entire protein (5,000 steps).

Ligand docking methods

Three chemical series of known antagonists (shown in Fig. 1) for CRF_1-R, the NBI compounds were docked to the apoprotein model of *h*CRF_1-R. The ligands were built with Maestro suite of software (Schrodinger, LLC, Portland, OR, 2006) and OPLS [36] charge in Maestro. A solvent of low dielectric (dielectric constant = 2.5) was used to mimic the interior of the GPCR TM barrel. For each ligand, all protonated states in the pH range 7 ± 2 were generated from Epik in Maestro and considered for docking.

We then performed ligand conformational sampling using the Monte Carlo sampling program in the *Macromodel* suite in *Maestro*. Each low energy ligand conformation was docked into the putative binding site using Glide standard precision docking (Glide SP). During docking, the torsion angles of the ligand were sampled as part of the Glide protocol. We found that generating multiple ligand conformations in MacroModel in conjunction with the limited torsional sampling of the ligand of Glide SP docking greatly expanded the conformational sampling of the ligand poses and led to enhanced docking efficiency. The receptor grid was generated with 50% scaled van der Waals radii for all receptor atoms. The docked conformations for each ligand from Glide were then sorted by buried surface area of the ligand. Also during docking the van der Waals radii of the ligand atoms were scaled by 50% in order to minimize steric clashes with protein side-chains. The docked ligand conformations with a buried surface area greater than 80% were selected for further processing. In each of the selected protein–ligand conformation, the residues within 5Å of the ligand were optimized using PRIME (Schrödinger) followed by minimization of the ligand with protein fixed. The binding energies were calculated as the difference of the ligand energy in protein minus the ligand energy in water. The ligand energy in water was calculated using the Generalized Born module in *Maestro*. The ligand poses from complexes were then clustered with a RMSD cutoff of 1Å and the top three clusters by binding energy were selected as final candidates. For each similar class of ligands, we also perturbed each compound to the other inside the binding pocket besides docking them independently following the procedure described above. The calculated binding energies of the top docked ligand poses were then compared with the experimental binding affinities for the three chemical series of CRF1 antagonists and the linear correlation coefficients were calculated. Among the top candidates, the ligand conformation that showed the best correlation with the experimental structure activity relationship (SAR) was selected as the final docked conformation.

LITiCon method: ligand Induced perturbations in the transmembrane rotational conformations (LITiCon)

LITiCon method has been discussed in detail earlier [26, 27]. Here we detail the steps of the method as applied to *h*CRF_1-R. We identified that TM helices 3, 4, 5, and 6 are in direct contact with NBI-27914 ligand and hence would undergo conformational changes due to ligand binding. We performed simultaneous systematic spanning of the rotational orientation of TM helices 3, 4, 5, and 6

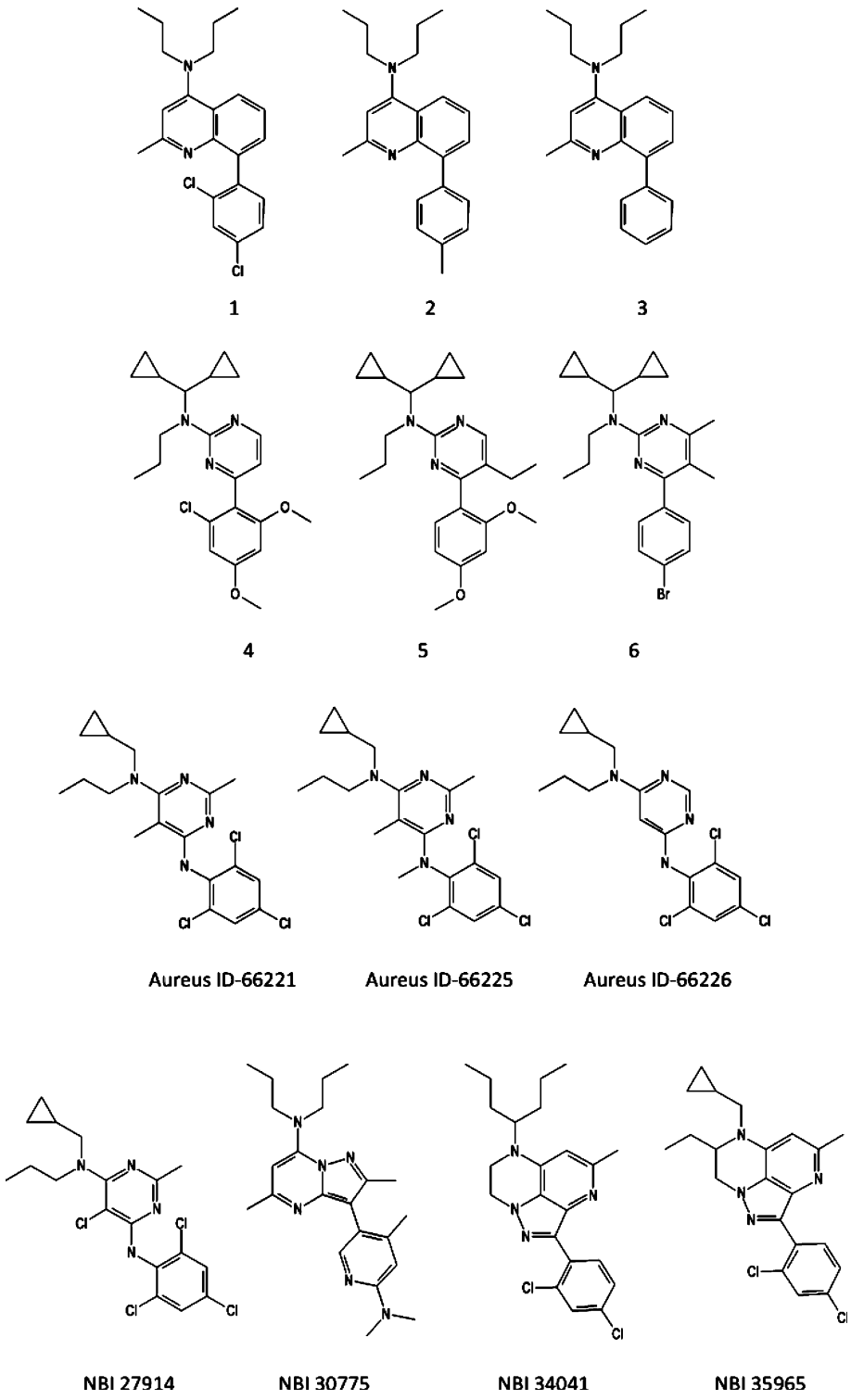

Fig. 1 Structures of $h\text{CRF}_1$-R antagonists modeled in this study

between ±40° in 10° increment with respect to the initial state. This process generated 9^4 (6,561) receptor conformations. For each conformation, the following steps were performed:

- Optimization of all side-chain conformations using SCWRL 3.0 [31].
- Conjugate gradient minimization of the potential energy of the ligand in the field of the rest of protein fixed until convergence of 0.3 kcal/mol-Å RMS deviation in force per atom is achieved.
- Calculation of the ligand binding energy defined as the difference of the potential energy of the ligand with

protein fixed, and the potential energy of the free ligand calculated in water using Generalized Born solvation method [37].
- Inter-helical and ligand-receptor hydrogen bonds using HBPLUS 3.0 [38].
- This generates a four dimensional binding energy landscape spanning between ±40° of the initial conformation. Next we identified all the local minima in this landscape and sorted them by total number of interhelical HB and ligand-receptor HB and then by binding energy. The final ligand stabilized receptor structural model was selected based on low binding energy and high number of HBs.

Results and discussion

Structural features of hCRF$_1$-R model as compared to other GPCRs

We examined the structural features such as helical kinks and the interhelical hydrogen bonds (HB) that stabilize the receptor conformation. P268 on TM4 is conserved among class B GPCRs, and makes a marked helical kink while another class B conserved P304 on TM5 does not cause a dominant kink in the ab initio model. This is in corroboration with the fact that that not all prolines present in the TM region cause a helical kink in membrane protein crystal structures [39]. The side chain of K343 (TM6) forms possibly a water mediated salt bridge with E238 on TM3. E238 and K343 are conserved across all class B secretin like GPCRs except that K343 is an Arg in some of the receptors. There is a network of polar residue interaction between TM3 and TM7. H228 on TM3 makes a long, perhaps a water mediated HB with E381 on TM7, which in turn makes a HB with N377 on TM7. This trail continues with E381 making a HB with Q384 on TM7, and Q384 makes a HB with N231 on TM3. Thus, we believe that TM3 and TM7 are tightly wound with the network of probably water mediated HB similar to the one found between TM6 and TM7 in rhodopsin inactive structure (pdb code: 1GZM) [40]. N231 and Q384 are conserved among secretin like class B GPCRs.

There are a significant number of aromatic stacking interactions between TM1, TM2 and TM3 similar to the class A peptide receptors like the chemokine receptors CCR1, CCR2, CCR3 and CCR5 [41, 42]. R194 on TM2 makes a cation–pi interaction with a network of aromatic residues H127 (TM1), W198 (TM2), F191 (TM2) and F227 (TM3). Y224 (TM3) pi stacks with the aromatic residues H228 (TM3), F232 (TM3) and F236 on TM3. H127, F191 are conserved in its aromatic character among the secretin like class B receptors. These stacking residues would confer stability to the receptor conformation.

Antagonist binding site and binding mode of the investigated compounds

We studied the binding sites of three chemical series of known antagonists [24, 25, 28, 43, 44] (shown in Fig. 1) for *h*CRF$_1$-R. Figure 2a–d show the docked conformations of **1**, **4**, NBI-27914 and NBI-30775 in *h*CRF$_1$-R, respectively (stereo representations are shown in Fig. S1 of supplementary material). All compounds have a central heterocyclic moiety with a branched secondary amine chain at one end and an aryl moiety on the other end. For all the compounds studied here, with the exception of **4–6** & NBI-30775, one of the nitrogen atoms on the central heterocyclic moiety is predicted to be protonated in the pH range 5.0-9.0 (pKa calculations were done using the Epik module in Maestro). In NBI-30775, the nitrogen on the terminal aryl moiety is protonated and not the central heterocyclic moiety. None of the nitrogen atoms in **4–6** are protonated at physiological pH. The predicted binding sites of all the compounds are located between TM3, TM4, TM5 and TM6 as shown in Fig. 2. Several residues in the binding site form key interactions with all the compounds studied here. These include H228 and F232 on TM3, M305 on TM5 and I354 on TM6. Using site directed mutagenesis, it was previously shown that mutation of H228 on TM3 and M305 on TM5 affect the binding of NBI-27914, NBI-30775, NBI-34041 and NBI-35965 compounds [14, 16]. In the current model, these two residues show favorable interactions with all the docked compounds. In the docked structures of **1**, NBI-27914 and NBI-30775, the protonated nitrogen in the central heterocyclic moiety forms a strong HB with H228 on TM3. The central heterocyclic moiety of compound **4** does not have a protonated nitrogen and it forms a weaker HB with H228 (2.8Å). In a previous study, mutating H228 to valine reduced the affinity of NBI-27914, but did not affect the binding of radiolabeled peptide agonist sauvagine [14]. Besides H228, the mutation of M305 on TM5 to Ile also showed significant effect on the affinity of NBI-27914 to inhibit the effect of radiolabeled sauvagine. In the predicted model, M305 makes hydrophobic contact with the ligands and the central heterocyclic moieties of the compounds also show favorable aromatic stacking with F232 on TM3. Both H228 and F232 show consistently strong interactions with all the docked compounds and are therefore the key contacts for binding of the compounds. Besides the residues on TM3 and TM5, I354 on TM6 shows a favorable hydrophobic contact with all the ligands.

In the *h*CRF$_1$-R, all compounds share a common binding pocket showing favorable interactions with several key

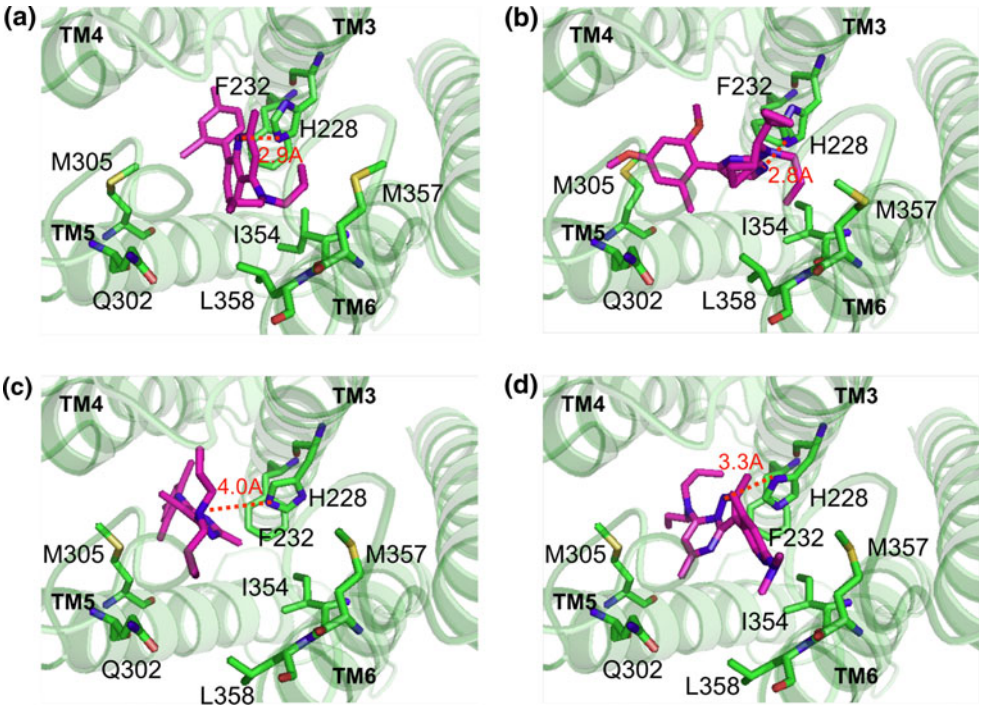

Fig. 2 Predicted binding sites of selected compounds in hCRF$_1$-R. Residues within 5Å of the ligand are shown in each figure. **a** Binding site for compound **1**; **b** compound **4**; **c** NBI-27914; **d** NBI-30775

residues as discussed in the previous paragraph. The magnitude of the interaction energy between these residues and the ligands vary depending on the structure of the compounds. In all the compounds, H228 shows the strongest interaction with the ligand, compared to the other residues in the binding pocket. However, the strength and nature of this interaction varies due to the chemical differences among the antagonists. H228 on TM3 forms a HB with all compounds except compound **4–6**. Since compounds **4–6** do not have a protonated nitrogen, H228 forms a HB with **4–6** and this interaction is 3 kcal/mol weaker than those with the other compounds. The interaction of M305 is 1–2 kcal/mol weaker with compounds **1–6** compared to the rest of the ligands. The predicted binding site of compounds **1–6** is closer to TM3 than TM5, whereas the binding sites of NBI-27914, -30775, -34041 and -35965 are closer to TM5. This leads to weaker interaction with M305 in **1–6**. Several residues in the binding cavity make contacts with specific ligands and are not present in the vicinity of the other compounds. L358 on TM6 makes contact with compounds **1–6** and this residue does not interact with the other ligands. The hydroxyl hydrogen of Y296 at the extracellular end of TM5 forms a HB with the central heterocyclic moiety in **4–6** and makes an aromatic contact with NBI-27914, NBI-30775, NBI-34041 and NBI-35965. Y296 shows a very weak interaction (<1 kcal/mol) with compounds **1–3**.

Figure 3a shows the extracellular half of the hCRF$_1$-R along with the small molecule binding site. The residues which have been shown to be important in CRF/CRF analog binding are highlighted in yellow [14, 45, 46]. Using site directed mutagenesis it was shown that the region V295-Y296-T297 (VYT) located at the extracellular end of TM5, when substituted with the corresponding residues of CRF2 receptor reduced the CRF induced cAMP accumulation by ten fold. The region T204-M205-S206-P207 (TMSP) at the extracellular end of TM2, when mutated to that of CRF$_2$-R did not show any effect, but together with the VYT mutation, reduced CRF induced cAMP accumulation by 100 fold [14]. In our modeled CRF$_1$-R structure, Y296 and T297 of the VYT region show favorable interactions with several NBI antagonists. Figure 3a shows the HB between Y296 and **4**. Figure 3b shows the position of Y296 relative to **1**, NBI-30775 and NBI-34041. T297 shows a moderately strong interaction with **4–6**. T297 is farther away from the binding site of the rest of the docked compounds and do not interact with them. Therefore, we find that the binding sites of CRF and the non-peptide small molecules slightly overlap one other since the residues Y296 and T297 are shown to interact with both sets of ligands.

Model for structure activity relationship for three chemical series of antagonists

We calculated the binding site and binding energies of several compounds shown in Fig. 1. Among these compounds, **1** is the best binder with an inhibition constant of 0.9 nM and has two chlorine atoms at the 2 and 4 positions on the benzene ring of the terminal aryl moiety as shown in

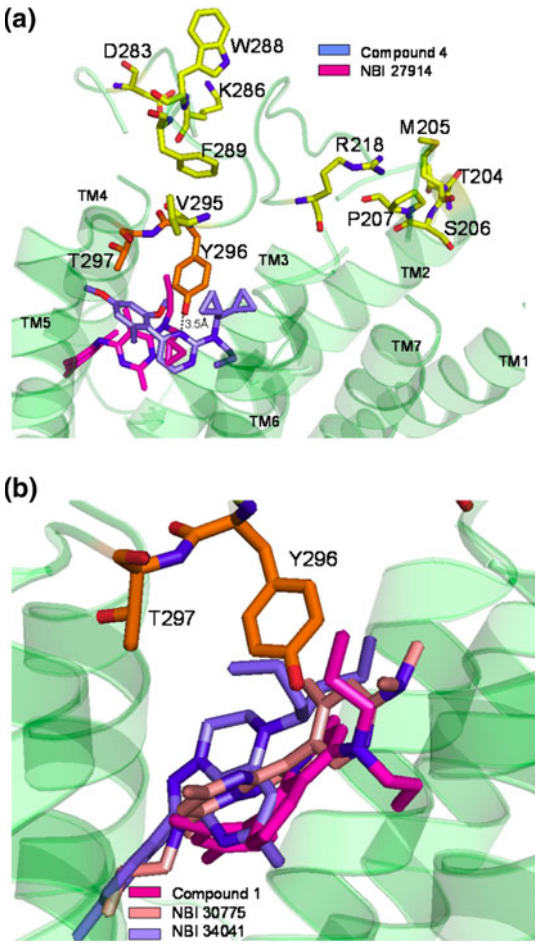

Fig. 3 **a** Extracellular half of the *h*CRF$_1$-R showing the binding sites of the compounds **4** and NBI-27914. The residues implicated in CRF or CRF analog binding are highlighted in *yellow*. The residues common to CRF and NBI compounds are shown in *orange*; **b** Location of Y296 and T297 relative to the compound **1**, NBI-30775, and NBI-34041

Fig. 1. Compound **2** has a methyl group at the 4 position and no chlorine group at the 2 position, and shows a lower binding affinity (32 nM) compared to compound **1**. In the predicted binding mode the interaction between compound **2** and the residues in the binding site (within 5Å) is 1.5 kcal/mol lower compared to that of **1**. The compound **3** has the worst binding affinity in this series of compounds, 420 nM. Compound **3** does not have any functional group on the terminal aromatic moiety (has hydrogens at 2 and 4 positions). In the predicted model, the interaction between **3** and the receptor is weaker compared to **1**. In both compounds **2** and **3**, the decrease in protein–ligand interaction is due to the reduced interaction of the ligand with several key residues in the binding cavity compared to compound 1. These residues are F232 and H228 on TM3, M305 on TM5 and L358 on TM6. F232, H228 and L358 showed a loss of 1.1, 1.5 and 0.3 kcal/mol in interaction energy respectively. M305 did not show a notable change in interaction energy. However, the side-chain of M305 in the docked conformations of **2** and **3** was 1.3Å away compared to **1**, which could lead to a weaker contact of M305 with **2** and **3**.

Among the second compound series from **4** to **6**, the best binder **4** has a binding affinity of 11 nM, which is worse compared to the best binder in the **1–3** series (compound **3**, 1 nM). Since the compounds in the **4–6** series do not have a protonated N, the HB with H228 is weaker (dipole–dipole interaction of non-protonated N) compared to that of the **1–3** series (charge-dipole interaction of protonated N). This explains the weaker binding affinity of the **4–6** series compared to the **1–3** series. The terminal aryl moiety in **4** has two methoxy groups at the 2 and 4 positions of the benzene ring and a chlorine group at the 6 position. In addition to this, compound **5** also has an ethyl group attached to the central heterocyclic moiety. Experimentally, compound **5** shows an 80-fold reduction in binding affinity (K_i = 860 nM) compared to **4**. In our predicted model, compound **5** shows lower protein–ligand interaction energy compared to **4** (1.5 kcal/mol lower). Due to the presence of the bulky ethyl group, the nitrogen atom of the central heterocyclic moiety is less accessible for HB. In our model, the HB between compound **5** and H228 is weaker compared to **4**. This leads to a lower binding affinity of **5** compared to **4**. In this series, compound **6** does not show good inhibition to the CRF$_1$ receptor. The compound **6** contains a single bromine atom at the 4 position on the terminal aryl moiety and two methyl groups on the central heterocyclic moiety. In our predicted model, **6** shows a significantly weaker interaction with the receptor compared to **1** (6 kcal/mol less compared to **1**). Compound **6** has no HB with H228 due to the presence of the bulky methyl groups on the central heterocyclic moiety, and therefore the loss of activity of **6**.

Here we analyze the structure–activity relationship of three analogs of the negative allosteric modulator NBI-27914. The structures of the studied analogs are given in Fig. 1. Figure 4a and b show the docked conformations of the three analogs and Fig. 4c shows the functional groups that are modified in the analog compounds. Groups G1 and G2 (as marked in Fig. 4) reside on the central heterocyclic moiety and G3 residues on the terminal aryl moiety. In NBI-27914, G1 is a methyl group and G2 is a chlorine atom while G3 is a hydrogen. In Aureus ID-66221 [28], the chlorine in G2 is replaced by a methyl group, while in Aureus ID-66225 [28], both G1 and G2 are methyl groups along with the addition of a new methyl group at the G3 position. In the analog Aureus ID-66226 [28], all the three groups, G1, G2 and G3 are hydrogens. The analog Aureus ID-66221 has a similar binding affinity as NBI-27914 (K_i: 2.3 nM for Aureus ID-66221 vs. 1.7 nM for NBI-27914) and we find that the ligand-receptor interaction energies of

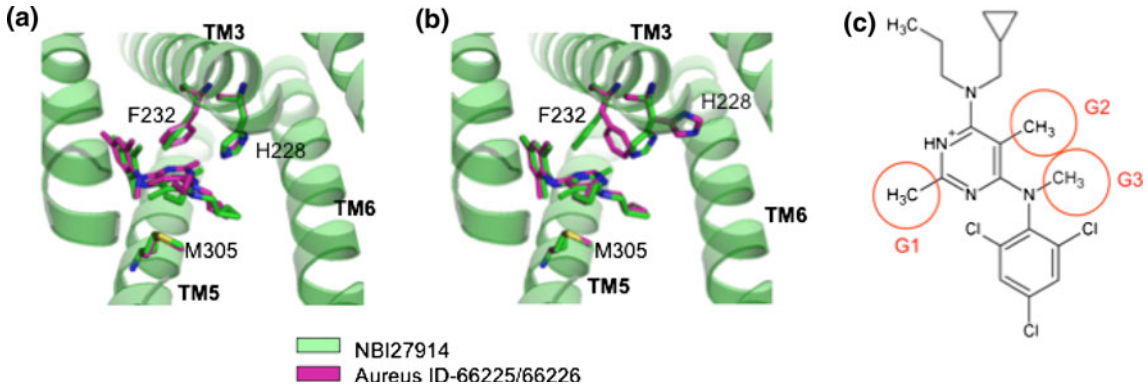

Fig. 4 Binding of NBI-27914 analogs to *h*CRF$_1$-R. **a** Binding site of NBI-27914 and Aureus ID-66225; **b** NBI-27914 and Aureus ID-66226; **c** structure of NBI-27914 scaffold showing the functional groups that were modified in the three analogs

NBI-27914 and Aureus ID-66221 are similar as well. Thus, replacing the chlorine atom with a methyl group (G1) has little effect on the binding of the compounds. In our predicted docked structures, the G1 faces the hydrophobic residues on TM4. Since the interaction between G1 and the receptor is hydrophobic in nature, replacing chlorine with a methyl group does not alter this interaction because chlorine and methyl groups have similar van der Waals radii (1.7Å). Addition of a methyl group on the terminal aryl moiety in Aureus ID-66225 leads to an 88 fold reduction in binding affinity compared to NBI-27914. In our predicted structure, Aureus ID-66225 shows a loss in protein–ligand interaction compared to NBI-27914. In the predicted structure, the terminal aryl moiety of NBI-27914 is close to M305 on TM5 (Fig. 4a). Placing a bulky methyl group on this moiety thus introduces steric clash between the ligand and M305. This, in concurrence with M305 shows the largest reduction in interaction with Aureus ID-66225 (2 kcal/mol) compared to NBI-27914. In NBI-66226, G1, G2 and G3 are all hydrogens and it shows three orders of magnitude reduction in binding affinity compared to NBI-27914. In the predicted model, the interaction energy of Aureus ID-66226 with the receptor is 6.4 kcal/mol less compared to that of NBI-27914 due to loss of contact of F232 and H228 (on TM3) with the ligand. In NBI-27914, the rotamer of F232 is packed in between the terminal aryl moiety and the G1 group (Fig. 4a). Once the G1 group is removed, F232 loses its contact with the ligand and assumes a relaxed rotamer configuration (Fig. 4b). As a result, the rotamer of H228, which is located near F232 also changes conformation and disrupts the HB with the ligand. By losing the strong electrostatic interaction with H228, Aureus ID-66226 shows a significantly weaker binding affinity to the CRF1 receptor compared to NBI-27914.

All the compounds studied here have similar structural motifs: i.e., a branched hydrocarbon motif followed by an aromatic/heterocyclic central moiety and a terminal aryl moiety. However, looking closely, there are many structural differences among these compounds including the central moiety, which can lead to significant differences in docked poses and hence protein–ligand interaction in the binding cavity. For example, the compound series **1–3** consist of a central double aromatic motif whereas the series **4–6** consist of a single aromatic ring with an aliphatic chain as the central moiety (Fig. 1). The compounds NBI-30775, 34041 and 35965 each consist of a 6 member pyridine ring fused with a 5 member pyrazole moiety. These ring structures pack differently with the aromatic residues of the receptor leading to different orientations of the ligands inside the binding cavity. The independently docked poses showed better correlations with the SAR and lower binding energies compared to the poses obtained by docking a single compound and then building the docked poses for the rest of the chemical series using the first compound as template. The independently docked ligand conformations also differed significantly from one another.

Thus, we find that the predicted model of the binding sites explain the structure activity relationship of three compound series in *h*CRF$_1$-R. The relative loss of binding energy for the three series of compounds is shown in table S1 of supplementary material.

Comparison of the predicted antagonist binding site to point mutation data

We calculated the change in the interaction energy of the ligand with the residues in the binding site (within 5Å) as a result of the point mutations at the residue location 305 of *h*CRF$_1$-R on the affinity of the NBI compounds. Using site directed mutagenesis, it has been shown that M305 interacts with many of the compounds studied here and mutating M305 to various hydrophobic residues has differential effect on the binding affinity of these compounds. Experimentally, M305 has been mutated to Ile, Val, Leu and Ala and M305I and M305V show the biggest decrease

in binding affinity for all the compounds [16]. This is in direct agreement with the predicted docked structures, where the decrease in protein–ligand interaction for the M305I mutant is the largest, 5.8 kcal/mol for NBI-27914, 4.1 kcal/mol for NBI-30775, 4.0 kcal/mol for NBI-34041 and 6.6 kcal/mol for NBI-35965. The reason for the large decrease in receptor-ligand interaction for the Ile mutant is the presence of a methyl group at the β carbon position of I305. In each of the four compounds, the methyl group on the M305 mutant introduces a steric clash with the central heterocyclic ring of the ligand. Unlike Ile, Leu does not possess an extra methyl group at the β carbon position. Thus, Leu preserves the van der Waals interaction of M305 with the ligand without introducing any steric repulsion. Therefore, the mutant M305L shows a relatively smaller decrease in protein–ligand interaction compared to the wild type receptor, 3.2 kcal/mol for NBI-27914, 2 kcal/mol for NBI-30775, 1 kcal/mol for NBI-34041 and 1.9 kcal/mol for NBI-35965.

Generalized pharmacophore for secretin family antagonists

Figure 5a shows the pharmacophore for non-peptide antagonists of hCRF$_1$, derived based on our docking results and experimental mutagenesis. All of the hCRF$_1$ antagonists studied in this work make contact with residues on TM3, TM5 and TM6 with the strongest interaction being the one with H228 on TM3. Besides H228, F232 on TM3 also shows consistently strong interaction with the hCRF$_1$

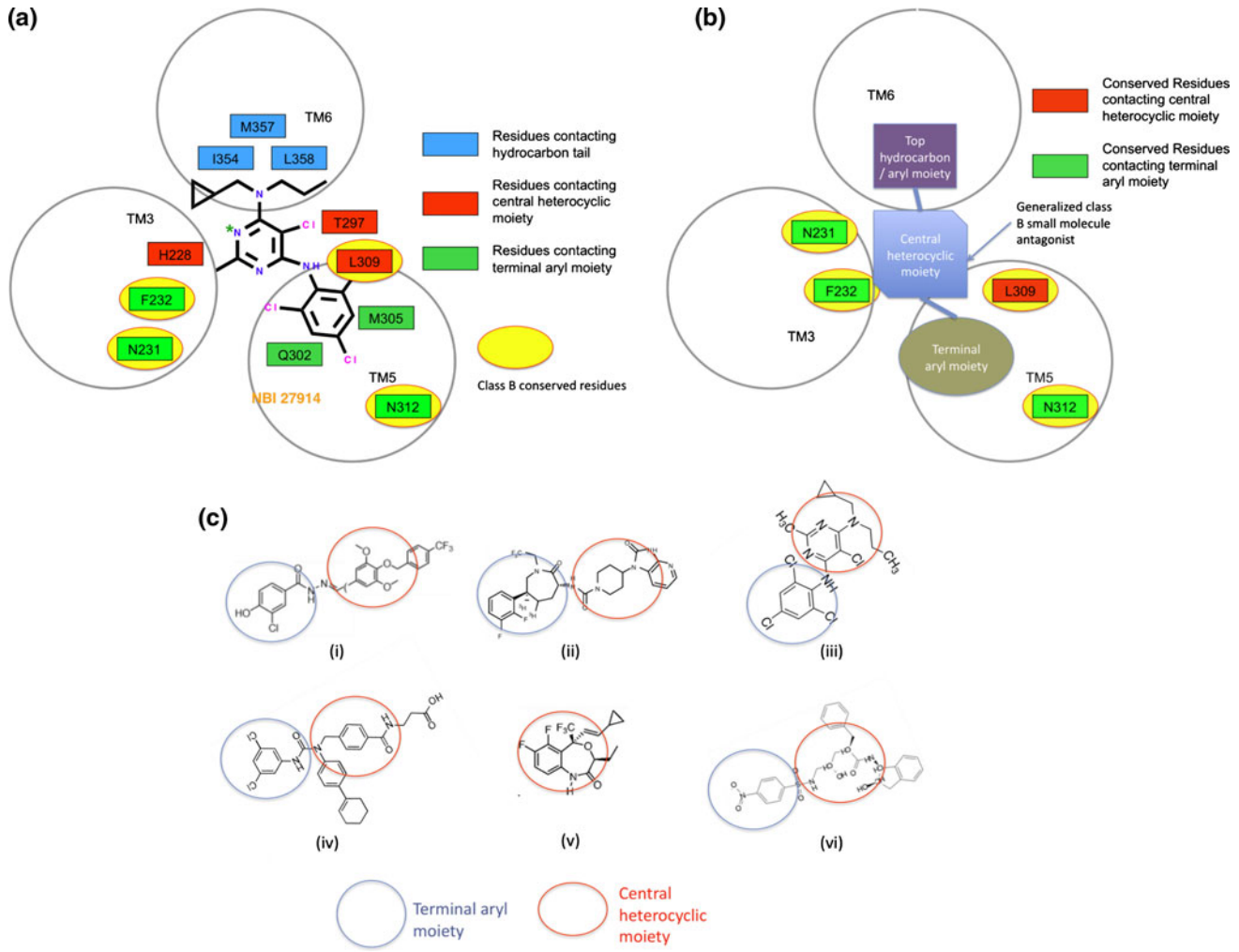

Fig. 5 **a** Pharmacophore for hCRF$_1$ antagonists. Residues are color-coded according to the ligand motif they contact. Conserved residues are marked with *yellow circles*. **b** Proposed generalized pharmacophore for class B small-molecule allosteric modulators. **c** Structures of several class B small molecule ligands. (*i*) Pituitary Adenylate Cyclase-Activating Polypeptide Receptor (PACAPR) [47], (*ii*) Calcitonin receptor (CALCR) [48], (*iii*) CRF1 antagonist NBI-27914, (*iv*) Glucose-Dependent Insulinotropic Polypeptide Receptor (GIPR) [49], (*v*) Parathyroid Hormone receptor (PTHR) [50], (*vi*) Vasoactive Intestinal peptide Receptor (VIPR) [51]. The common structural motifs in these compounds, that show resemblance with CRF1 antagonists are highlighted

antagonists. Among the TM5 residues, the interaction of M305 with the antagonists has been discussed in previous sections. Besides, L309 shows moderately strong interactions with the central heterocyclic moiety while Q302 and N312 interact with the terminal aryl moiety of the antagonists. Residues, which contact the hydrocarbon tail of the antagonists, are I354, M357 and L358 on TM6. We next investigated whether the pharmacophore for the CRF1 antagonists could be used to provide insight into the allosteric binding pockets found in other class B GPCRs. The motivation for this comes from the fact that, among class A GPCRs, the biogenic amine receptors show similar residue contacts for agonists and antagonists and the ligands binding to these receptors also have similar structural motifs (e.g., positively charged amine group at one end and an aromatic/aryl moiety at the other end). CRF1 is a member of the secretin family of receptors (class B, subclass B1) and in recent years non-peptide modulators have been discovered for several receptors in this family [47–51]. The structures of several non-peptide modulators of class B1 family are shown in Fig. 5c. Comparing the structures of these ligands, we find that all of the ligands share a terminal aryl moiety and a central heterocyclic moiety similar to the CRF1 antagonists. Therefore it is possible that the binding pockets among the class B receptors share common patterns of residue contacts that identify the similar structural motifs found in these ligands. The members of the secretin family of receptors show moderate sequence identity in the transmembrane regions (sequence alignment given as supplementary material). In TM3, H228 which is predicted to form hydrogen bonds with the charged groups of the CRF1 antagonists is not conserved within the CRF family. However, N231 which is located close to H228, is conserved throughout the secretin family. This residue could form HB with charged/polar groups of non-peptide ligands in the other class B receptors. Next to N231 is another class B conserved residue F232, which forms a π-stacking with the terminal aryl moieties of the CRF1 antagonists and stabilizes the aryl groups within the binding pocket. This terminal aryl group is present in several other class B modulators except the one for CALCR, where a triple ring structure is present instead of an aryl moiety, and the one for PTHR, where the terminal group is missing altogether. Thus, the conserved residue F232 could play a role in the binding of other class B modulators by interacting with the terminal aryl moieties. Among the TM5 residues that contact the CRF1 antagonists, L309 and N312 are conserved among the class B receptors. In our models, N312 interacts with the terminal aryl moieties of the CRF1 antagonists while L309 contacts the central heterocyclic moieties. Therefore, we propose that these two residues could interact with the corresponding moieties in the other class B modulators. In TM6, the residues I354, M357 and L358 are partially conserved among the class B receptors. I354 and M357 show conservative replacements in all the sequences except GLP1R (T instead of I) and PACAPR (T instead of M), respectively, while L358 shows conservative replacement in all the sequences. In our model, these three residues interact with the terminal hydrocarbon moieties of the CRF1 antagonists. This terminal hydrocarbon moiety is not strictly conserved among other class B modulators, where sometimes an aromatic group is present instead of a branched alkane (e.g., antagonists for PACAPR and VIPR) or polar groups as in the antagonist for GLPR. Thus, it is difficult to predict the nature of residue contacts in this region for other class B antagonists. However, the heterogeneous nature of the TM sequences in this region suggests that TM6 could play a role in imparting selectivity to the binding of the class B modulators. Based on the discussion so far, we have presented a generalized pharmacophore for non-peptide class B receptor modulators shown in Fig. 5b. A generalized pharmacophore will be important in studying the binding of known class B modulators and also for designing ligands, where small molecule modulators are not known, such as the secretin receptor.

Ligand Induced conformational changes in hCRF$_1$-R upon binding of NBI-27914

Figure 6a shows the original docked conformation of NBI-27914 and the ligand stabilized conformation obtained from *LITiCon* (stereo views are shown in Fig. S2 of supplementary material). The ligand stabilized conformation incorporates the conformational changes that were directly induced by the ligand on the receptor. The helices TM3, TM4, TM5 and TM6 that are in direct contact with NBI-27914 undergo these conformational changes that are directly induced by the ligand. Using *LITiCon*, we predicted small rotational movements in these TMs, which improved the interactions of the neighboring residues with the ligand by 4 kcal/mol compared to the original receptor conformation. Figure 6b shows the binding energy landscape for NBI-27914 docked to the *h*CRF$_1$-R. For ease of representation, a two dimensional section of the multidimensional binding energy landscape is shown. Since TM3 and TM5 undergo the largest conformational changes upon NBI-27914 binding, these two helices are chosen as principal or the conformational coordinates of the two dimensional binding energy landscape. The binding energy landscape shows three favorable degenerate binding energy wells along the TM5 rotation axis, corresponding to different conformations of TM5. The energy minimum at $-40°$ rotation of TM5 is well separated from the energy minimum at $+10°$ by 20 kcal/mol barrier, while the energy minimum at $+40°$ rotation of TM5 is close to the one at 10°

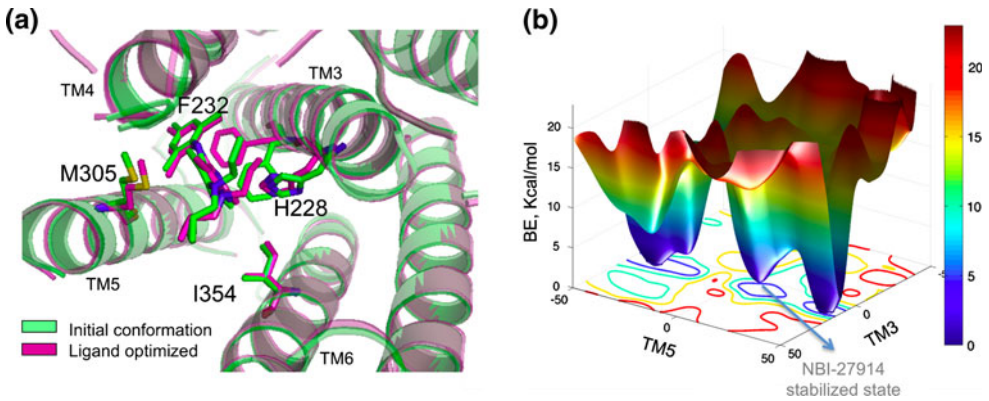

Fig. 6 **a** Comparison of the apo receptor structure of hCRF$_1$-R to the NBI-27914l stabilized hCRF$_1$-R structure from LITiCon. **b** Binding enthalpy landscape of NBI-27914 docked to hCRF$_1$-R. Since the actual binding energy landscape is multidimensional, a 2D section of the landscape is shown. The *axes* represent conformational changes in TM3 and TM5. The *blue regions* show favorable energy and red regions show unfavorable energy. The predicted ligand stabilized state is marked in the figure

minimum (marked in Fig. 6b). The energy minimum at 10° in the center improves the contact between the ligand and M305 by bringing the M305 side chain closer to the ligand, while the other two minima takes M305 further away from the ligand. The central minimum thus satisfies the experimental mutation data and was chosen as the ligand stabilized state. The energy minimum at +40° could be another antagonist bound conformation while the energy minimum at −40° well separated by a barrier, represents a receptor state inaccessible to NBI-27914. In recent studies, two categories of hCRF$_1$-R antagonists were identified, one which suppressed CRF binding as well as G-protein mediated *c*AMP accumulation, while the other class of compounds enhanced CRF binding but suppressed *c*AMP accumulation [19]. This class of compounds also enhanced basal activity of the receptor in an over-expressed cell assay and thus could stabilize a weakly active state of the receptor. In our simulations, the energy minima at −40° could represent this weakly active state stabilized by hCRF$_1$-R allosteric antagonists. For strong inverse agonists such as NBI-27914, this active state is inaccessible due to the large energy barrier. However, this barrier could be lowered by the binding of allosteric modulators such as NBI-77173, that are proposed to stabilize the weakly active state. Binding of antagonists or inverse agonists always separates the inactive state from the active state by a barrier [24, 25]. The slight positive rotation of TM3 moved H228 closer to the protonated nitrogen of NBI-27914, thereby strengthening the HB with the ligand. The side chain of F232, which was previously near the central heterocyclic ring of the ligand now moved closer to the terminal aromatic moiety and formed a favorable aromatic interaction with the ligand. Compared to the other helices, TM6 showed smaller changes and did not affect the binding site notably. The ligand induced optimization of the receptor structure led to the rearrangement of several HB networks among the TM helices. In the original model of the hCRF$_1$ receptor, Y224 on TM3 forms a HB with E281 on TM7. NBI-27914 induces a conformational change in TM3 that causes this HB to break, presumably compensating this loss of interaction by gaining in the HB between the ligand and H228 on TM3. Another rearrangement in interhelical HBs is observed near the intracellular ends of TM4 and TM3. In the original receptor model, K257 (TM4) makes a HB with the backbone oxygen of Y241 (TM3). In the ligand optimized conformation, this HB is broken and a new HB is formed between the side chains of C262 (on TM4) and Y241 (TM3). The side chain of K257 (TM4) forms a new HB with the backbone oxygen of L248 on intracellular loop 2.

Virtual ligand screening results on CRF$_1$-R structural models

To test the utility of the hCRF$_1$-R models for identifying potent compounds, we have performed a virtual ligand screening (VLS) on the hCRF$_1$-R structural models before and after *LITiCon*. The ligand database consists of 10,000 randomly picked compounds from the NCI database and 3290 small molecules from a GPCR specific dataset (from TimTech). This database was then seeded with 347 known hCRF$_1$-R potent compounds and 774 hCRF$_1$-R non-potent compounds. The hCRF$_1$-R non-potent compounds are structurally similar to the potent compounds but having low binding affinity in hCRF$_1$-R (Ki or $IC_{50} > 2$ μM). The rationale for including the non-potent compounds is to test whether the VLS procedure can identify the potent compounds out of the non-potent decoy ones, which are structurally similar to the hCRF$_1$-R potent compounds. Figure 7 shows the enrichment of hCRF$_1$-R potent compounds as function of filter cutoff. Enrichment is defined as follows:

$$\text{Enrichment} = \frac{\text{Number of CRF}_1\text{ hits at a given cutoff}}{\text{Expected number of CRF}_1\text{ hits assuming a uniformly random distribution}}$$

Figure 7a shows the enrichment in the original *h*CRF_1-R conformation and Fig. 7b shows the same in the NBI-27914 stabilized *h*CRF_1-R *LITiCon* conformation. In the original *h*CRF_1-R conformation, an enrichment of 2.5 is observed at 10% cutoff. The highest enrichment of 3.0 is obtained at a cutoff of 23%. In contrast, the NBI-27914 stabilized conformation shows a highest enrichment of 3.6 obtained at a cutoff of 10%. Comparing Fig. 7a and b, the NBI-27914 stabilized *h*CRF_1-R conformation shows an improved overall enrichment with respect to the original *h*CRF_1-R conformation. We also examined if the VLS procedure yields the stronger enrichment for the strong binders compared to the weak binders in the list of *h*CRF_1-R positive compounds. Figure 7 also shows the enrichments for the strong binders (defined as K_i or $IC_{50} < 100$ nM) and the weak binders (100 nM $< K_i$ or $IC_{50} < 2$ μM). For the original *h*CRF_1-R conformation, at a 10% cutoff, the enrichment for the best binders is 2.3 and 4.0 for the weak binders. For the NBI-27914 stabilized conformation (at the same cutoff), the enrichment for the best binders is 3.6 and that for the weak binders is 3.3. Therefore, the original *h*CRF_1-R conformation shows less enrichment for the strong binders and more enrichment for the weak binders, whereas the NBI-27914 stabilized conformation shows the opposite trend, higher enrichment for the strong binders and less enrichment for the weak binders. *Therefore, using LITiCon for modeling the ligand stabilized state of the receptor leads to a better enrichment for the hCRF*$_1$*-R potent compounds and also sequester the more potent compounds instead of the weaker hits.*

The efficiency of a VLS run is also measured by simultaneous maximization of the true positives (TP) and the minimization of the number of false negative (FN) compounds within the same percentage cutoff. Therefore, we calculated the true positives within a certain cutoff, false negatives within the cutoff, and false positive (FP), which is the percentage of *h*CRF_1-R potent compounds beyond the designated cutoff (the rejected part of the VLS list) and true negative (TN), which is the percentage of CRF1 negative compounds beyond the designated cutoff. In order to achieve an optimum filtering, TP and TN should be high and FP and FN should be low. Figure 8 shows the variation of these four quantities with cutoff for the NBI-27914 stabilized CRF_1 conformation. At low cutoff, TP and FP are low and they increase with increasing cutoff. TN and FN are initially high and they decrease to zero at high cutoffs. Therefore, the optimum cutoff range is between 15% and 50%, where both TP and TN are above 50 and FP and FN are below 50. Therefore, although the maximum enrichment is observed at a cutoff of 10%, efficient filtering is achieved at a cutoff of 15% or more for the NBI-27914 stabilized conformation.

Although the CRF1 potent compounds are structurally similar, they have markedly different binding affinities. Thus, the antagonist stabilized CRF1 model is able to distinguish the strong binders from the weak ones where

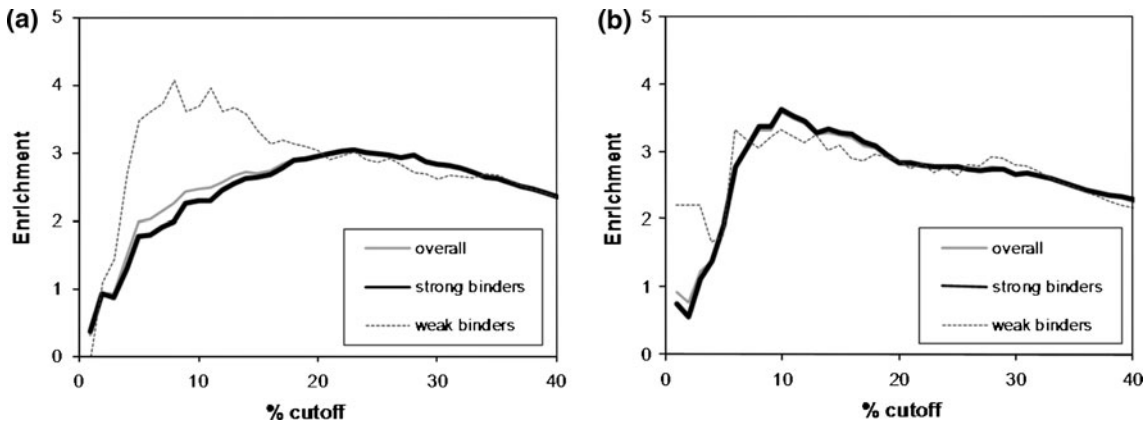

Fig. 7 Comparison between enrichments obtained from two different *h*CRF_1-R conformations; **a** original conformation used in docking the compounds in Fig. 1; **b** *h*CRF_1-R conformation stabilized by NBI-27914. The figures show the overall enrichment and the ones for weak and strong binders

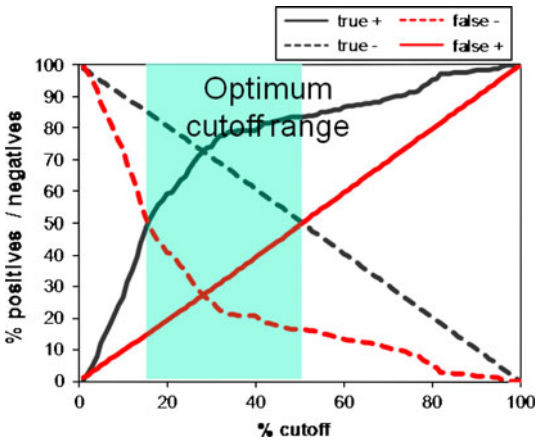

Fig. 8 TP, TN, FP and FN as functions of cutoff for the NBI-27914 stabilized receptor conformation. *Green region* indicates the zone of optimum cutoff (for efficient filtering)

both the strong and the weak binders are structurally similar. In drug design, lead optimization involves identifying the strongest binding compounds from a set of closely related chemical analogs. Thus, besides identifying new drug targets, our model could also be used in developing a lead from a hit compound.

Conclusions

We modeled an ensemble of conformational states for the hCRF$_1$-R using ab initio modeling MembStruk method that is independent of alignment with class A GPCRs. In addition we have shown that ligand induced conformational changes in hCRF$_1$ receptor are important in the design of small molecule antagonists for hCRF$_1$-R. Potent inhibitors such as NBI-27914 bind in the transmembrane region between TM3, TM5 and TM6. Residues H228 and F232 on TM3, and M305 TM5 and L358 on TM6 anchor the aromatic groups in the ligand, and contribute the most to the interaction with NBI-27914. The modeled binding sites and the calculated ligand receptor interaction energies for the various derivative compounds of NBI-27914 are in agreement with the measured change in IC50 for these compounds. We have also studied the binding sites of six other antagonists shown in Fig. 1. The calculated binding energies are consistent with the measured IC50 for these compounds. The ligand induced conformational change leads to movement of TM3 and TM5 that results in a 4 kcal/mol improvement in binding to NBI-27914. The binding energy surface shows possible multiple minima in the antagonist stabilized state. We have shown that it is possible to have more than one inactive state and that the possible receptor active state is well separated from the inactive state by an energy barrier. In a VLS study using the models, we have shown that the ligand stabilized receptor conformation shows a 44% increase in enrichment in high affinity compounds compared to the model that is not optimized for ligand induced conformational changes. In these results we have demonstrated that the ligand stabilized conformational state plays an important role in designing antagonists for hCRF$_1$-R.

Acknowledgments The authors thank Sanofi-Aventis for providing funding to N.V.'s group for this project.

References

1. Kehne J, De Lombaert S (2002) Non-peptidic CRF1 receptor antagonists for the treatment of anxiety, depression and stress disorders. Curr Drug Targets CNS Neurol Disord 1:467–493
2. Holsboer F (2001) CRHR1 antagonists as novel treatment strategies. CNS Spectr 6:590–594
3. Smagin GN, Dunn AJ (2000) The role of CRF receptor subtypes in stress-induced behavioural responses. Eur J Pharmacol 405:199–206
4. Zobel AW, Nickel T, Kunzel HE, Ackl N, Sonntag A, Ising M, Holsboer F (2000) Effects of the high-affinity corticotrophin-releasing hormone receptor 1 antagonist R121919 in major depression: the first 20 patients treated. J Psychiatr Res 34: 171–181
5. Ising M, Zimmermann US, Kunzel HE, Uhr M, Foster AC, Learned-Coughlin SM, Holsboer F, Grigoriadis DE (2007) High-affinity CRF1 receptor antagonist NBI-34041: preclinical and clinical data suggest safety and efficacy in attenuating elevated stress response. Neuropsychopharmacol 32:1941–1949
6. Martinez V, Tache Y (2006) CRF1 receptors as a therapeutic target for irritable bowel syndrome. Curr Pharm Des 12:4071–4088 and references cited therein
7. Zorrilla EP, Koob GF (2004) The therapeutic potential of CRF1 antagonists for anxiety. Expert Opin Investig Drugs 13:799–828
8. Palczewski K, Kumasaka T, Hori T, Behnke CA, Motoshima H, Fox BA, Le TI, Teller DC, Okada T, Stenkamp RE, Yamamoto M, Miyano M (2000) Crystal structure of rhodopsin: a G protein-coupled receptor. Science 289:739–745
9. Cherezov V, Rosenbaum DM, Hanson MA, Rasmussen SG, Thian FS, Kobilka TS, Choi HJ, Kuhn P, Weis WI, Kobilka BK, Stevens RC (2007) High-resolution crystal structure of an engineered human beta2-adrenergic G protein-coupled receptor. Science 318:1258–1265
10. Jaakola VP, Griffith MT, Hanson MA, Cherezov V, Chien EY, Lane JR, Ijzerman AP, Stevens RC (2008) The 2.6 Angstrom crystal structure of a human A2A adenosine receptor bound to an antagonist. Science 322:1211–1217
11. Warne T, Serrano-Vega MJ, Baker JG, Moukhametzianov R, Edwards PC, Henderson R, Leslie AG, Tate CG, Schertler GF (2008) Structure of a beta1-adrenergic G-protein-coupled receptor. Nature 454:486–491
12. Park JH, Scheerer P, Hofmann KP, Choe HW, Ernst OP (2008) Crystal structure of the ligand-free G-protein-coupled receptor opsin. Nature 454:183–187
13. Schlyer S, Horuk R (2006) I want a new drug: G-protein-coupled receptors in drug development. Drug Discov Today 11:481–493
14. Liaw CW, Grigoriadia DE, Lorang MT, De Souza EB, Maki RA (1997) Localization of agonist- and antagonist-binding domains of human corticotropin-releasing factor receptors. Mol Endocrinol 11:2048–2053

15. Hoare SR, Sullivan SK, Schwarz DA, Ling N, Vale WW, Crowe PD, Grigoriadis DE (2004) Ligand affinity for amino-terminal and juxtamembrane domains of the corticotropin releasing factor type 1 receptor: regulation by G-protein and nonpeptide antagonists. Biochemistry 43:3996–4011
16. Hoare SRJ, Brown BT, Santos MA, Malany S, Betz SF, Grigoriadis DE (2006) Single amino acid residue determinants of non-peptide antagonist binding to the corticotropin-releasing factor1 (CRF1) receptor. Biochem Pharmacol 72:244–255
17. Urban JD, Clarke WP, von Zastrow M, Nichols DE, Kobilka B, Weinstein H, Javitch JA, Roth BL, Christopoulos A, Sexton PM, Miller KJ, Spedding M, Mailman RB (2007) Functional selectivity and classical concepts of quantitative pharmacology. J Pharmacol Exp Ther 320:1–13
18. Kobilka BK, Deupi X (2007) Conformational complexity of G-protein-coupled receptors. Trends Pharmacol Sci 28:397–405
19. Hoare SRJ, Fleck BA, Gross RS, Crowe PD, Williams JP, Grigoriadis DE (2008) Allosteric ligands for the corticotropin releasing factor type 1 receptor modulate conformational states involved in receptor activation. Mol Pharmacol 73:1371–1380
20. Heo J, Han SK, Vaidehi N, Wendel J, Kekenes-Huskey P, Goddard WA III (2007) Prediction of the 3D structure of FMRF-amide neuropeptides bound to the mouse MrgC11 GPCR and experimental validation. Chem Biochem 8:1527–1539
21. Hall S (2005) Development of a structure prediction method for G-Protein coupled receptors. Caltech PhD Thesis http://etd.caltech.edu/etd/available/etd-06012005-235052/
22. Vaidehi N, Floriano WB, Trabanino R, Hall S, Freddolino P, Choi EJ, Zamanakos G, Goddard WA III (2002) Structure and function prediction for G-Protein coupled receptors. Proc Natl Acad Sci USA 99:12622–12627
23. Li Y, Zhu F, Vaidehi N, Goddard WA III, Sheinerman F, Reiling S, Morize I, Mu L, Harris K, Ardati A, Laoui A (2007) Prediction of the 3D structure and dynamics of human DP G-protein coupled receptor bound to an agonist and an antagonist. J Am Chem Soc 129:10720–10731
24. Chen C, Wilcoxen KM, Huang CQ, Xie YF, McCarthy JR, Webb TR, Zhu YF, Saunders J, Liu XJ, Chen TK, Bozigian H, Grigoriadis DE (2004) Design of 2, 5-dimethyl-3-(6-dimethyl-4-methylpyridin-3-yl)-7-dipropylaminopyrazolo[1, 5-a]pyrimidine (NBI 30775/R121919) and structure–activity relationships of a series of potent and orally active corticotropin-releasing factor receptor antagonists. J Med Chem 47:4787–4798
25. Gross RS, Guo Z, Dyck B, Coon T, Huang CQ, Lowe RF, Marinkovic D, Moorjani M, Nelson J, Zamani-Kord S, Grigoriadis DE, Hoare SRJ, Crowe PD, Bu JH, Haddach M, McCarthy J, Saunders J, Sullivan R, Chen T, Williams JP (2005) Design and synthesis of tricyclic corticotropin-releasing factor-1 antagonists. J Med Chem 48:5780–5793
26. Bhattacharya S, Hall SE, Vaidehi N (2008) Agonist-induced conformational changes in bovine rhodopsin: insight into activation of G-protein-coupled receptors. J Mol Biol 382:539–555
27. Bhattacharya S, Hall SE, Li H, Vaidehi N (2008) Ligand-stabilized conformational states of human b_2 adrenergic receptor: insight into G-protein-coupled receptor activation. Biophys J 94:2027–2042
28. Chen C, Dagnino R Jr, De Souza EB, Grigoriadis DE, Huang CQ, Kim KI, Liu Z, Moran T, Webb TR, Whitten JP, Xie YF, McCarthy JR (1996) Design and synthesis of a series of non-peptide high-affinity human corticotropin-releasing factor1 receptor antagonists. J Med Chem 39:4358–4360
29. Trabanino RJ, Hall SE, Vaidehi N, Floriano WB, Goddard WA III (2004) First principles predictions of the structure and function of G-protein coupled receptors: validation for bovine rhodopsin. Biophys J 86:1904–1921
30. Schertler GFX (1998) Structure of rhodopsin. Eye 12:504–510
31. Canutescu AA, Shelenkov AA, Dunbrack RL Jr (2003) A graph-theory algorithm for rapid protein side-chain prediction. Prot Sci 12:2001–2014
32. Lim KT, Brunett S, Iotov M, McClurg RB, Vaidehi N, Dasgupta S, Taylor S, Goddard WA III (1993) Molecular dynamics for very large systems on massively parallel computers: the MPSim program. J Comput Chem 18:501–521
33. Mayo SL, Olafson BD, Goddard WA III (1990) DREIDING-a generic force field for molecular simulations. J Phys Chem 94:8897–8909
34. MacKerell AD, Bashford D, Bellott M, Dunbrack RL, Evanseck JD, Field MJ, Fischer S, Gao J, Guo H, Ha S, Joseph-McCarthy D, Kuchnir I, Kuczera K, Lau FTK, Mattos C, Michnick S, Ngo T, Nguyen DT, Prodhom B, Reiher WE, Roux B, Schlenkrich M, Smith JC, Stote R, Straub J, Watanabe M, Wiorkiewicz-Kuczera J, Yin D, Karplus M (1998) All-atom empirical potential for molecular modeling and dynamics studies of proteins. J Phys Chem B 102:3586–3616
35. Fiser A, Do RK, Sali A (2000) Modeling of loops in protein structures. Prot Sci 9:1753–1773
36. Jorgensen WL, Maxwell DS, Tirado-Rives J (1996) Development and testing of the OPLS all-atom force field on conformational energetics and properties of organic liquids. J Am Chem Soc 118:11225–11236
37. Zamanakos GA (2001) Fast and accurate analytical method for the computation of solvent effects in molecular simulations. PhD thesis Caltech, Pasadena
38. McDonald IK, Thornton JM (1994) Satisfying hydrogen bonding potential in proteins. J Mol Biol 238:777–793
39. Hall SE, Roberts K, Vaidehi N (2009) Position of helical kinks in membrane protein crystal structures and the accuracy of computational prediction. J Mol Graph Model 27:944–950
40. Li J, Edwards PC, Burghammer M, Villa C, Schertler GFX (2004) Structure of bovine rhodopsin in a trigonal crystal form. J Mol Biol 343:1409–1438
41. Hall SE, Mao A, Nicolaidou V, Finelli M, Wise EL, Nedjai B, Kanjanapangka J, Harirchian P, Chen D, Selchau V, Ribeiro S, Schyler S, Pease JE, Horuk R, Vaidehi N (2009) Elucidation of binding sites of dual antagonists in the human chemokine receptors CCR2 and CCR5. Mol Pharmacol 75:1325–1336
42. Vaidehi N, Schlyer S, Trabanino RJ, Floriano WB, Abrol R, Sharma S, Kochanny M, Koovakat S, Dunning L, Liang M, Fox JM, de Mendonca FL, Pease JE, Goddard WA III, Horuk R (2006) Predictions of CCR1 chemokine receptor structure and BX 471 antagonist binding followed by experimental validation. J Biol Chem 281:27613–27620
43. Huang CQ, Wilcoxen K, McCarthy JR, Haddach M, Webb TR, Gu J, Xie Y-F, Grigoriadis DE, Chen C (2003) Synthesis and SAR of 8-arylquinolines as potent corticotrophin-releasing $factor_1$ (CRF_1) receptor antagonists. Bioorg Med Chem Lett 13:3375–3379
44. Huang CQ, Grigoriadis DE, Liu Z, McCarthy JR, Ramphal J, Webb T, Whitten JP, Xie MY, Chen C (2004) Design, synthesis, and SAR of 2-dialkylamino-4-arylpyrimidines as potent and selective corticotrophin-releasing $factor_1$ (CRF_1) receptor antagonists. Bioorg Med Chem Lett 14:2083–2086
45. Assil-Kishawi I, Abou-Samra AB (2002) Sauvagine cross-links to the second extracellular loop of the corticotropin-releasing factor type 1 receptor. J Biol Chem 277:32558–32561
46. Gkountelias K, Tselios T, Venihaki M, Deraos G, Lazaridis I, Rassouli O, Gravanis A, Liapakis G (2009) Alanine scanning mutagenesis of the second extracellular loop of type 1 corticotropin-releasing factor receptor revealed residues critical for peptide binding. Mol Pharmacol 75:793–800
47. Beebe X, Darczak D, Vadis-Taber RA, Uchic ME, Scott VE, Jarvis MF, Stewart AO (2008) Discovery and SAR of hydrazide

antagonists of the pituitary adenylate cyclase-activating polypeptide (PACAP) receptor type 1 (PAC1-R). Bioorg Med Chem Lett 18:2162–2166
48. Moore EL, Burgey CS, Paone DV, Shaw AW, Tang YS, Kane SA, Salvatore CA (2009) Examining the binding properties of MK-0974: A CGRP receptor antagonist for the acute treatment of migraine. Mol Cell Pharmacol 602:250–254
49. Kodra JT, Jorgensen AS, Andersen B, Behrens C, Brand CL, Christensen IT, Guldbrandt M, Jeppesen CB, Knudsen LB, Madsen P, Nishimura E, Sams C, Sidelmann UG, Pederson RA, Lynn FC, Lau J (2008) Novel glucagon receptor antagonists with improved selectivity over the glucose-dependent insulinotropic polypeptide receptor. J Med Chem 51:5387–5396
50. Carter PH et al (2007) Discovery of a small molecule antagonist of the parathyroid hormone receptor by using an N-terminal parathyroid hormone peptide probe. Proc Natl Acad Sci USA 104:6846–6851
51. Chu A, Caldwell JS, Chen YA (2010) Identification and characterization of a small molecule antagonist of human $VPAC_2$ receptor. Mol Pharmacol 77:95–101